Even *EPJ Techniques and Instrumentation* (2015) 2:17
DOI 10.1140/epjti/s40485-015-0027-5

EPJ Techniques and Instrumentation
a SpringerOpen Journal

REVIEW Open Access

"The Even-Lavie valve as a source for high intensity supersonic beam"

U. Even

Correspondence: even@post.tau.ac.il
Sackler School of Chemistry, Tel Aviv University, Tel Aviv, Israel

Abstract

We use extensive computer simulation to design (and test) a high pressure, fast acting, pulsed, valve that can produce short pulses of gas. We use flow simulations from shaped nozzles to optimize the beam density and finally use low density simulation to decide on the best skimmer shape and placement. All these details are crucial to operate a high intensity beam machine.

Introduction

The art of supersonic beams has advanced since its early years [1–6], when simple cw sources were used. The main limitation on achieved beam intensity was set by the pumping capacity of the source chamber- mainly large diffusion pumps and Roots pumps (with capacities of 3.000-10.000 liter/second). It was realized that when the background pressure was too high in the source chamber, beam propagation was diminished, and careful adjustment in the skimmer design was required to avoid the generated barrel shock wave and Mach disk structure [7–9] (Fig. 1).

These limitations were overcome when pulsed gas sources became available [10–16]. If the gas pulse is short enough (shorter than a typical molecular reflection time from the walls of the vacuum chamber), and if the repetition rate is low enough to so that the mean gas pressure is less than 10^{-5} mbars in the source chamber, then the gas expands without hindrance, and no structured shock waves interfere with the jet propagation. Much smaller turbo-molecular pumps (300–500 l/sec) can now be used for low repetition rate experiments (10-50Hz), while bigger pumps (3000 l/sec) are still required for higher repetition rates (1–5 KHz) pulsed valve systems. The following parts will summarize our experience with one type of a pulsed valve that we developed, and is still the only one that can be used over a very wide temperature scale (4^0-550^0 K). The valve is an electro- magnetic actuated device. Readily available computer simulation programs can now be used to optimize the electro- magnetic structure, the mechanical movement dynamics, the nozzle shape and the interaction of the high density resulting jet with skimmers. These processes will be explained and experimental results will be shown. These valves, known as the "Even-Lavie" valves are now widely used in more than 100 labs. Some details have been published before [17].

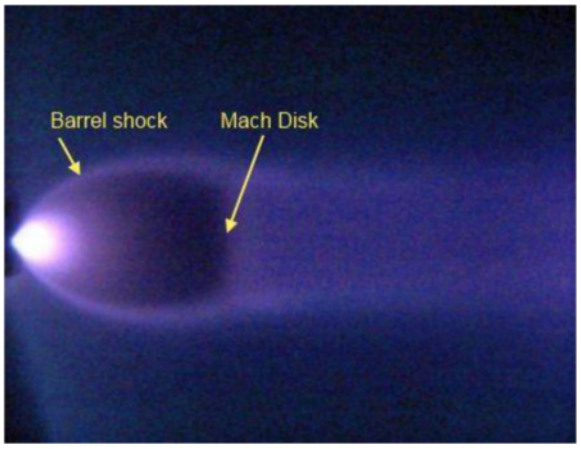

Fig. 1 CW gas jet expanding from sonic nozzle into poor vacuum (from [60]) showing the shock wave structure in jets. Barrel shock wave, Mach disk and the "Zone of silence [7]" between them are clearly visible in this rare photograph. The gas was made to glow by electron beam excitation

High pressure, wide temperature range pulsed valve

General dimensions consideration and material selection

There are several possibilities in generating a pulse valve to create high intensity jets. Some of them are obvious and some need careful choice of materials and geometries.

1. We want the gas pulse to be short enough to reduce the required pump load and to allow the gas to expand into a good vacuum and neglect vacuum walls interaction during the pulse. Considering the high velocity of a light expansion gas (and Helium will be proven to be the best choice, with velocities of up to ~2300 m/sec at 500°K), and typical dimension of 0.1 m for the vacuum wall diameter, we get a gas reflection time of 40 microseconds. The gas pulse should be shorter than this typical time.
2. The short pulse time can be achieved by miniaturization of the moving parts (small masses), creating a magnetic structure with small air gaps (to maximize the generated field and force) and to minimize the amplitude of the mechanical movement.
3. The coil generating the field should have small inductance to allow for a fast rise time of the current pulse (microseconds).
4. The wide temperature range implies that there will be considerable thermal expansion in the valve components. Not all the materials in the valve have the same expansion coefficients, thus the method of sealing should be based on constant force applied by internal springs to compensate for thermal expansion.
5. We should strive to make the metallic parts inert dictating the use of stainless steel (304) for the valve body, high nickel alloy for the springs (Nimonic 90), and strong strength alloy (Inconel 625) for the thin walled pressure tube. The magnetic parts are made from a magnetic stainless steel (alloy 250) which is a compromise between the required high magnetic saturation alloy and sensitivity to corrosion (usually these two requirements are contradictory). Not all batches of the magnetic circuit alloys are created equal, depending on their history of thermal treatment. We have to test (and reject) each batch for its magnetic

saturation by inserting it in a coil and measuring the resultant current flow, selecting only the batch with high permeability in high magnetic fields. The sealing material is Kapton that is flexible enough but also strong enough for the sealing forces required and can also withstand elevated temperatures.

Magnetic circuit simulation

We tested several possible configurations to generate the required fields for the short pulses required. The simulation results of the magnitude of the magnetic field is shown in Fig. 2. We use the Lorenz magnetic simulation program, using the rotational symmetric two dimensional program [18].

To keep the moving plunger mass to a minimum (0.2gr) and minimize the forces acting on the thin walled pressure tube (containing the high pressure gas) we kept the inner diameter to ~ 3 mm. The 6 layers copper coil has an inductance of only 4 micro-henry, which combined with its low resistance (<0.2 ohm) allows for a rise time of the current pulse to be short (20 μsec.). The generated magnetic force between the moving plunger and its static magnetic plug is high (~10 N) to allow the rapid closure of the gap, and recoil with high velocity to its original sealing position. The position of the plunger, or the exiting gas flow, does not follow the current shape as will be explained. A soft (3 N) spring (not shown) keeps the plunger in its sealing, normally closed position. To operate the valve one needs to switch a voltage of 24 volts, causing a current of 15–20 amps in the coil, for about 20 μsec. (see Fig. 3). The valve opening requires low energy, of ~ 6 mili-joule per pulse, so operating at 500Hz causes a heating of 3 Watts which has to be carried away.

Mechanical motion simulation

The mechanical motion of the plunger due to the current pulse in the coil is far from trivial. There are several factors influencing the motion:

1. The masses of the plunger and the return spring.
2. The shape of the current pulse.
3. The local saturation of the magnetic properties of the plunger and plug.
4. The closure of the air gap in the magnetic circuit during the motion.

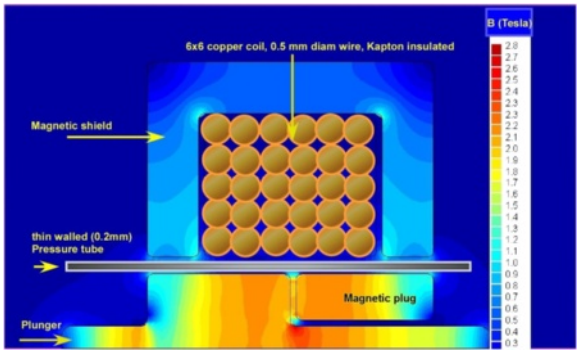

Fig. 2 The Magnitude of the magnetic field created by a 15 amps current in the coil is mapped. The magnetic plunger and its counter plug insert are separated by 0.1 mm only. The magnetic field in the gap (~2 Tesla) is enough to cause deep magnetic saturation in the plunger and plug. Displayed is the upper half of the rotationally symmetric geometry

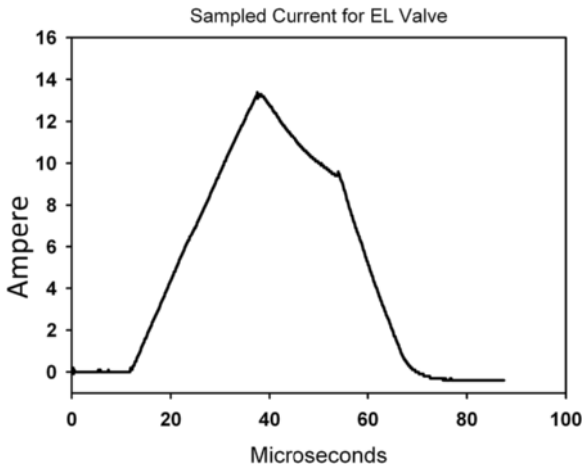

Fig. 3 Current pulse shape in the valve coil

5. The recoil velocity when the plunger hits the immobile plug.
6. The recoil from the nozzle surface at the end of the motion cycle.

Solving the equation of motion under all of these variables is complicated and several simplifications are needed. We used the free simulation program Scilab to solve the differential equation of motion [19]. We assumed that the force acting on the plunger is triangular, that upon collision with the plug or front surface a velocity reversal occurs, and that the flow through the nozzle is proportional to the plunger opening to the power of two (the exposed area of the nozzle to the flow). One point is evident: If the plunger is driven by too high current in the coil, multiple pulses of gas will result, because of the recoil in its movement. The simulation also predicts that the valve will be fast enough and that typical gas pulses of 25 μsec. are possible. We were encouraged that experimental tests [20] verified these simulations and are shown in Figs. 4 and 5.

The valve can be operated between a single pulse to 500Hz. The background pressure shows a linear rise with frequency indicating that all the pulses are the same. When

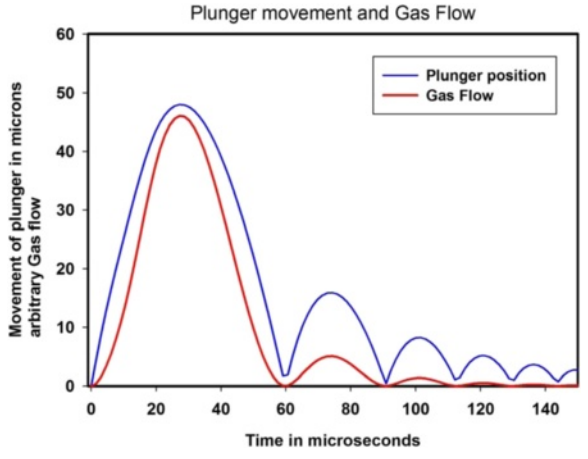

Fig. 4 Plunger movement and gas flow are simulated by solving the equation of motion under simplifying assumption

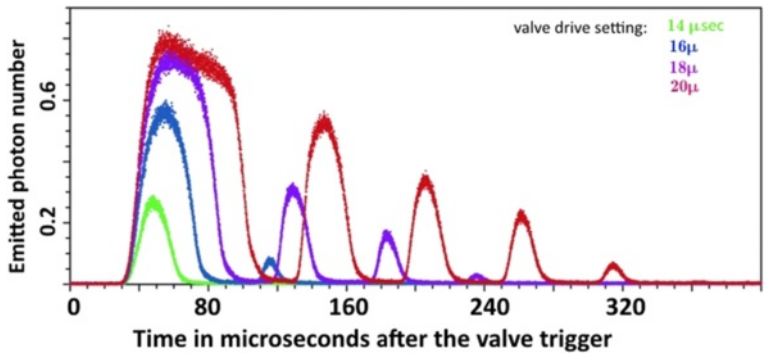

Fig. 5 Measured valve response to varying excitation pulse amplitudes reprinted from [20]

trying to raise the frequency above that limit a deviation occurs, and the gas consumption shows several mechanical resonances (at 640, 830, and 940 Hz). That is why we feel that reliable operation is limited at f < 550Hz. Operating at higher frequency is possible, with multiple pulses for each trigger pulse (Fig. 6).

Valve construction details

The moving parts are displayed in Fig. 7. The magnetic alloy plunger can move to close a narrow gap (0.05 mm) in the magnetic circuit when a pulse of current flows in the outside coil. The gas is contained inside a narrow walled non-magnetic tube (Inconel). The movement of the plunger is guided by two Ruby cylindrical slide bearings. The tolerances on the dimensions here are crucial (0.005 mm.) to ensure repeatable movement over billions of pulses without lubrication.

The internal mechanism is sealed at both ends by Kapton discs by pressing with a strong spring against the end and front flanges as can be seen in Fig. 8. The strong spring force allows for both over pressure relief and thermal expansion dimensional changes when the valve temperature is varied over a wide range.

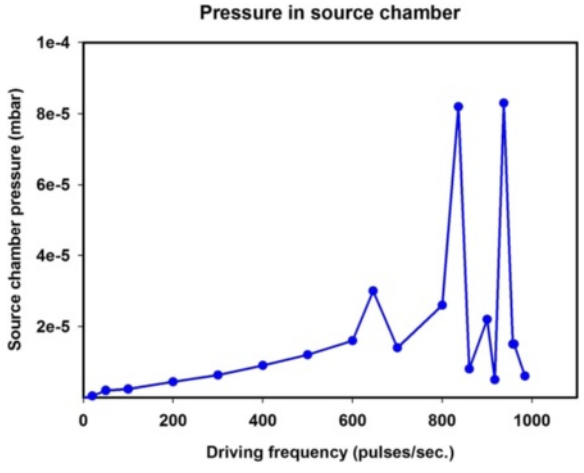

Fig. 6 Source chamber pressure as a function of repetition pulse rate

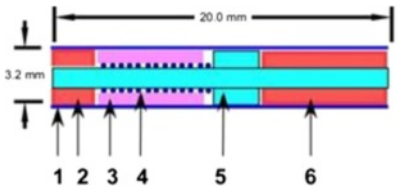

Fig. 7 Internal mechanism details

1. Stainless gas inlet tube (1/16”).
2. Tightening spring (100 N) and pressure relief valve.
3. Kapton foil gasket (rear, 0.125 mm. thickness).
4. Ruby rear guiding ferrule.
5. Return spring (Nimonic 19 alloy).
6. Thin walled pressure vessel (Inconel 625 alloy).
7. Reciprocating plunger (magnetic stainless steel alloy 750).
8. Kapton insulated copper coil (0.6 mm wire diameter 6x6 winding).
9. Magnetic shield (alloy 17/4PH) and field concentrator.
10. Ruby front guiding ferrule.
11. Kapton foil gasket (front, 0.125 mm. thickness).

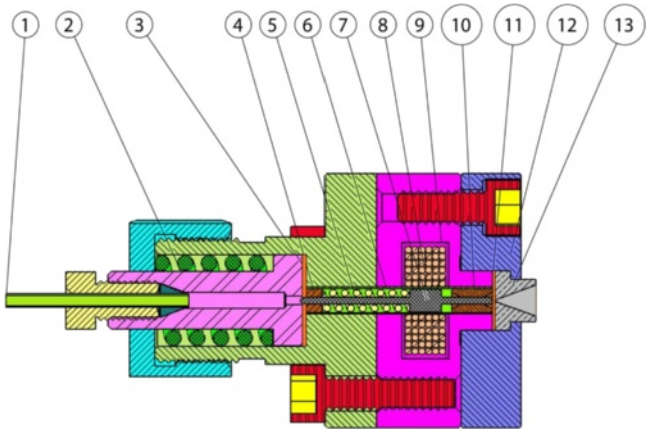

1. Stainless gas inlet tube (1/16”).
2. Tightening spring (100N) and pressure relief valve.
3. Kapton foil gasket (rear, 0.125 mm. thickness).
4. Ruby rear guiding ferrule.
5. Return spring (Nimonic 19 alloy).
6. Thin walled pressure vessel (Inconel 625 alloy).
7. Reciprocating plunger (magnetic stainless steel alloy 750).
8. Kapton insulated copper coil (0.6 mm wire diameter 6x6 winding).
9. Magnetic shield (alloy 17/4PH) and field concentrator.
10. Ruby front guiding ferrule.
11. Kapton foil gasket (front, 0.125 mm. thickness).
12. Front flange (stainless or copper).
13. Conical (or trumpet) shape expansion nozzle (Zirconia ceramic or hardened stainless steel).

Fig. 8 Room Temperature valve cross section

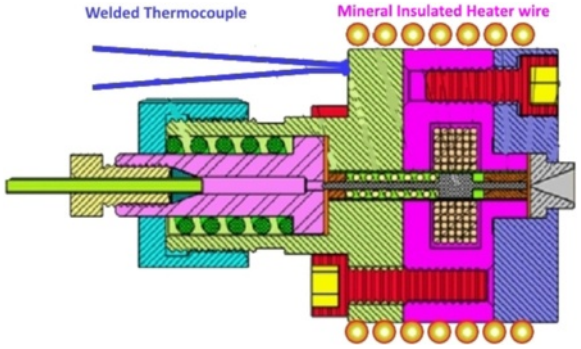

Fig. 9 High temperature valve construction

12.Front flange (stainless or copper).
13.Conical (or trumpet) shape expansion nozzle (Zirconia ceramic or hardened stainless steel).

The carrier gas is exposed to Inconel, Stainless steel of various grades and Kapton only, and is thus inert to most molecules. It is susceptible to metallic corrosion if Halides are used and the Kapton is sensitive to Ammonia or other Amines. Low concentration (1 %) of Halides (even Fluorine) can be compatible if water traces are removed. Low concentration of Amines can also be tolerated, but may require more frequent gaskets change. We recommend that the valve should be pumped down when not in use (say overnight) so as to reduce the corrosion rate (even with water vapors).

The heated version of the valve (up to 250^0c) is similar in its construction to the room temperature valve but with the addition of mineral insulated heater wire and a thermocouple welded to the valve body (Fig. 9). The upper temperature limit is set by the Kapton seals polymer and coil wire insulation. The closely coupled heater and thermocouple ensure short thermal response time (minutes) and a suitable temperature controller should be used. Some means to dissipate the heat in the valve upon cooling should be provided to shorten the cooling time. The high temperature operation allowed us to cool large molecules to less than 1°K [21].

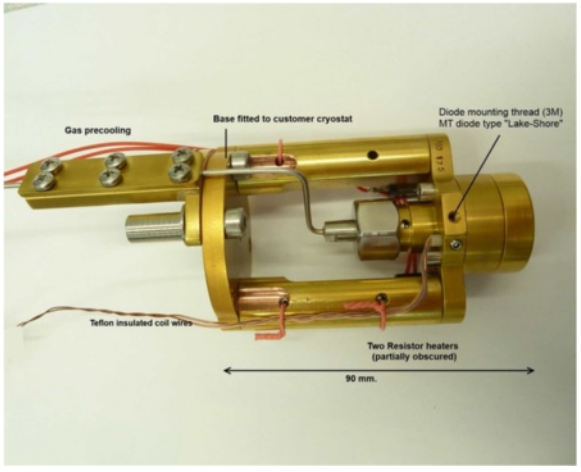

Fig. 10 Temperature controlled Cryogenic valve

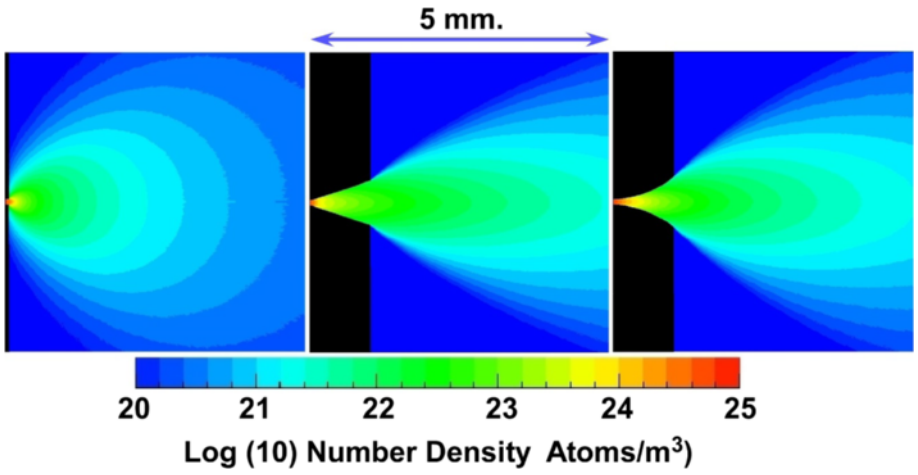

Fig. 11 Number density maps for three nozzle shapes: sonic, cone and trumpet. Expansion from 1 bar of Helium of 0.1 mm nozzle opening

The cryogenic valve version is again similar in its construction, but the valve body is made of copper, which is softer than stainless and should be carefully handled. To prevent corrosion in air the copper is coated with TiN thin layer. The temperature sensor is a Si diode. These valves can operate over the temperature range of 5^0-400°K continuously without mechanical adjustments (that plague other designs). At low temperature the coil electrical resistance drops down so a lower driver current is required, keeping the self-heating to a minimum. A cryo cooler with 6 Watts cooling power is required if working at 500Hz. These valves have produced Helium droplets of up to 10^9 atoms [22–24]. Careful control of the temperature is required (better than 0.1^0 k) because cluster size is very temperature sensitive (Fig. 10).

Nozzle design

Early days nozzles were mainly pinhole (or sonic) nozzle. They are simple to make and produce diffuse (non-collimated) beams with limited cooling capabilities. The adiabatic

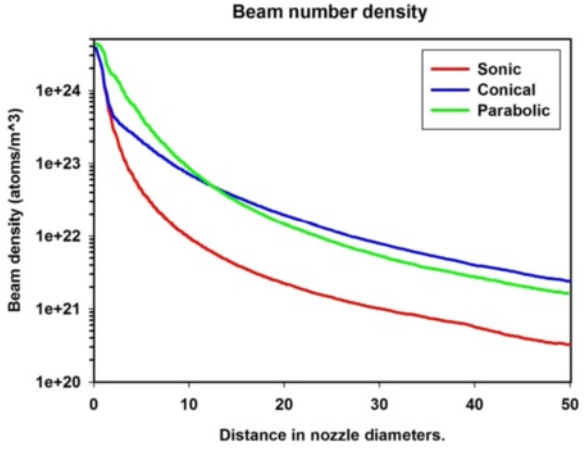

Fig. 12 Density drop with distance from the nozzle for the three geometries. At large distances of the shaped nozzle beam density is ~10 times greater than the sonic nozzle

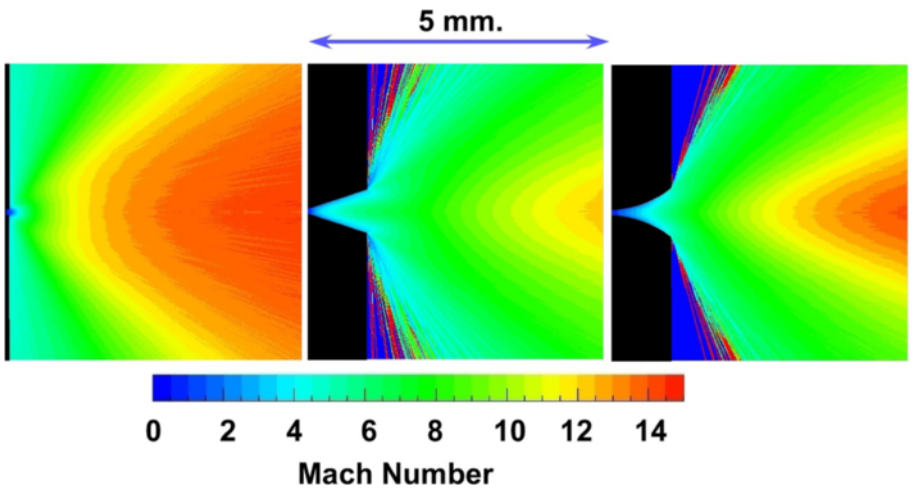

Fig. 13 Mach number Maps for the same three nozzles

expansion of the gas can be analytically solved and easily computed either by CFD [25, 26] calculation (solving the Navier–Stokes equation) or simulated using a variety of Monte-Carlo programs. It was soon realized that shaping the nozzle can shape the expanding gas jet [3, 26–29] and change the number of collisions before the beam density drops to low value and the expansion and cooling practically "Freezes" [8, 9, 30]. Most nozzles have small length dimensions (several mm in size due to pumping limitations) and making a complicated and smooth shape is difficult [31]. We chose to study a series of simple conical shaped nozzles that are relatively easy to make [28]. We used a freely available DSMC program [32] to simulate the nozzle flow for various shape (opening angle) nozzles. The program runs on a PC and takes several hours to run. It is practically limited to a stagnation density of roughly 0.1-1bars, but the mean free path is so much smaller than the nozzle dimension that we believe the results can be extrapolated to a much higher pressure with simple density scaling. The results of the simulation were effective in designing an optimally shaped conical nozzle in terms of high on axis beam density and cooling (Mach

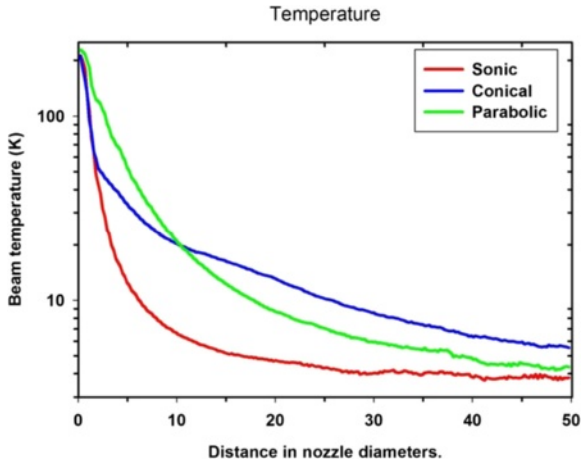

Fig. 14 Beam temperature drop with distance from the nozzle for the three shapes. The cooling continues beyond 50 nozzle diameters, and the parabolic nozzle shape wins

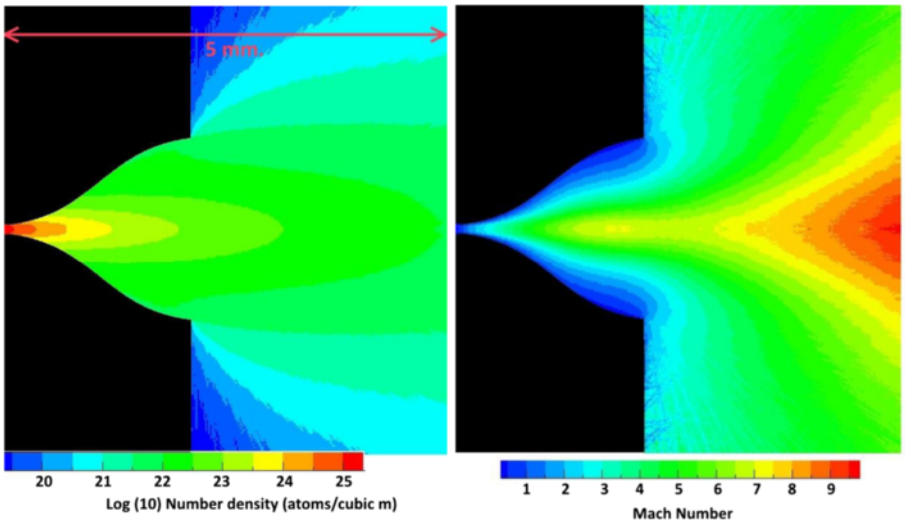

Fig. 15 Number density and Mach number for a bell shaped nozzle

number). In the following figures we show the expanding jet from three different 0.1 mm nozzles: pinhole nozzle, 40° full angle conic nozzle and a "trumpet" (parabolic) shaped nozzle. Both densities and Mach number are plotted (Fig. 11)

The beam created by the sonic nozzle is wide and its density drops sharply with the distance. A more collimated beam is generated by the 40° full angle conical nozzle and a similar density map is generated by the trumpet shaped nozzle. Figure 12 shows the axial density drop with the distance (measured in nozzle diameters):

The slow drop with distance for the shaped nozzle will result in a larger number of collisions before the expansion "Freezes", translated in colder beam. This is seen in Figs. 13 and 14.

We simulated the expansion from more elaborate, and difficult to machine, shaped nozzle. While higher on axis beam density can be achieved (better beam collimation), the beam temperatures are usually higher too (~10°K). One such example is shown in

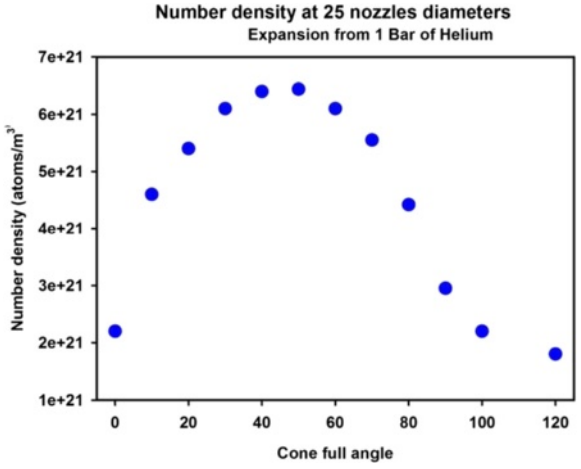

Fig. 16 Beam Density for various nozzle opening angles

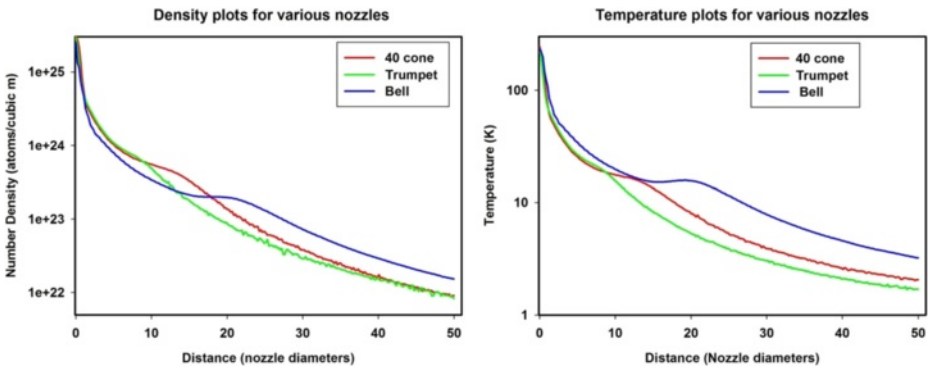

Fig. 17 Density and Temperature plots for the three nozzle shapes: Cone, Trumpet and Bell

Fig. 15 where a bell shaped nozzle (common to many rocket engines) that approximates in its behavior the well-known Laval nozzle [33]:

If we concentrate on (the simple to manufacture) conical nozzles, than the next question is what is the best opening angle for the cone? Both sonic nozzle (180^0 angle) and channel nozzle (0^0) will produce similar jets with rapid decline of the axial beam density and a small number of collisions before the expansion "freezes". Comparing the on axis beam number density for various nozzle opening angles, we can see (Fig. 16) that an optimum exists for angles of 40–60° (full cone angle). The optimum depends on the simulation model namely on what one assumes for the boundary layer on the cone face. Technically one has to assume an "accommodation coefficient" for the atom colliding with the cone surface [34] (a parameter that indicates how much of the energy have been lost to the surface). We assumed a full accommodation for the wall collisions. This is probably a severe assumption for a highly polished surface with a light carrier gas (Helium). Varying the accommodation coefficient in the simulation varies the optimum angle by about 10° from the optimum.

A comparison of the density and temperature drop with distances is presented in Fig. 17 for the three nozzle shapes: 40 deg. Cone, Trumpet (parabolic) and Bell shape.

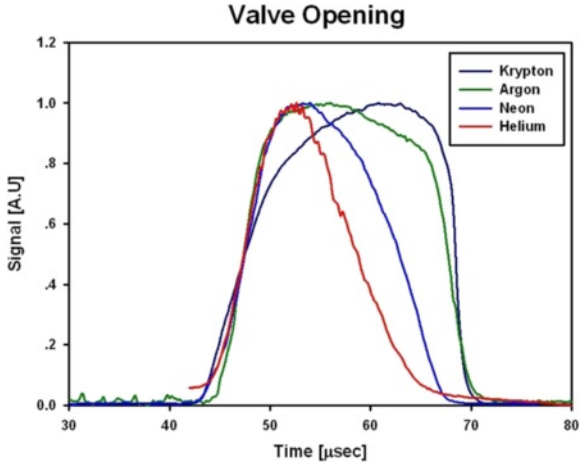

Fig. 18 Emitted pulse durations for various expanding gases

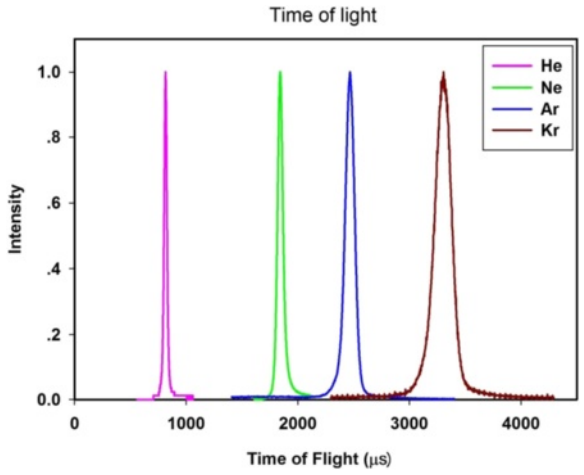

Fig. 19 Time of flight for metastable atoms (1.4 m flight tube). Stagnation temperature is 300 K and pressure is 50 bar

The reflected shock waves inside the nozzle are evident in the kink from the smooth curve, most evident in the bell shaped nozzles. The smoothest curve is achieved for the trumpet shaped nozzle.

Beam properties

Pulse profile in time at the valve exit

The gas flow is time limited by the mechanical movement as described above. The actual pulse of gas leaving the valve was measured by a fast ion gauge and is shown in Fig. 18 for various noble gas. The same plunger movement (constant pulse driving) causes different pulse shape due to the finite flow time of the gas in the valve. The heavier gasses (with their lower molecular velocities and higher viscosities) create slower and wider pulses.

These measurements also indicate that a pulse time width of ~10microsec. is a practical lower limit for pulsed valves of this type and dimensions.

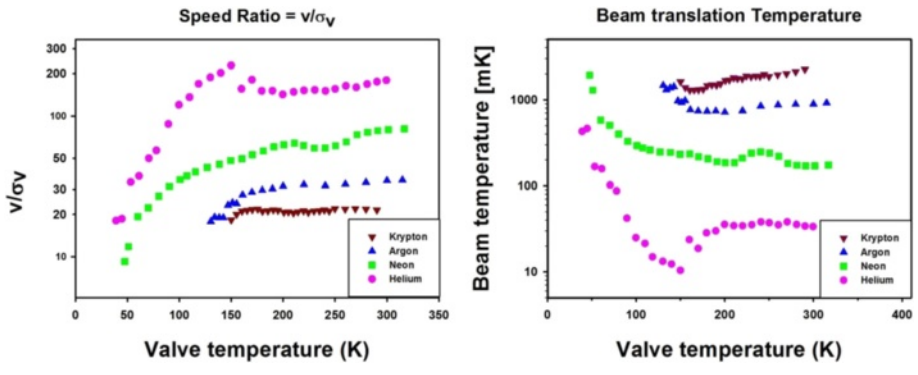

Fig. 20 Speed ratio and attained temperature for various gases

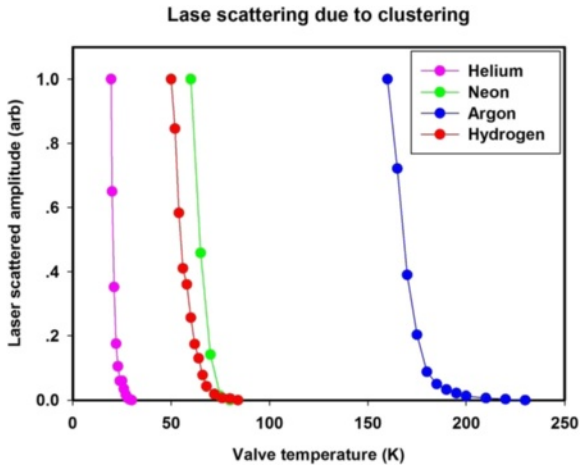

Fig. 21 Scattered laser light, indicating extensive cluster growth below specific temperatures for each expansion gas

Velocity spread and achieved Mach numbers and temperatures

The short puff of gas emitted by the valve is moving at high velocity in the axial direction (1750 m/s for helium from a room temperature valve). The achieved velocity uniformity is quite high (1 % or better) so the axial dimension expands slowly as the gas moves in the vacuum, the faster atoms move to the front and the slower ones arrange themselves at the back. The spread in the radial direction is much faster, even when collimated by skimmers. The arrangement in the axial direction according to the velocity allows to select velocities according to their arrival time [35–38], achieving very high kinetic energy resolution. The flight times of electrically excited (neutral) atoms are shown in Fig. 19.

From the data in Fig. 19 we can construct the average velocity v and the velocity spread sv (standard deviation of the velocity distribution) and from these two value construct the velocity ratio $S = v/sv$ (Mach number). We can estimate the beam temperature from these numbers [6, 8] (Fig. 20)

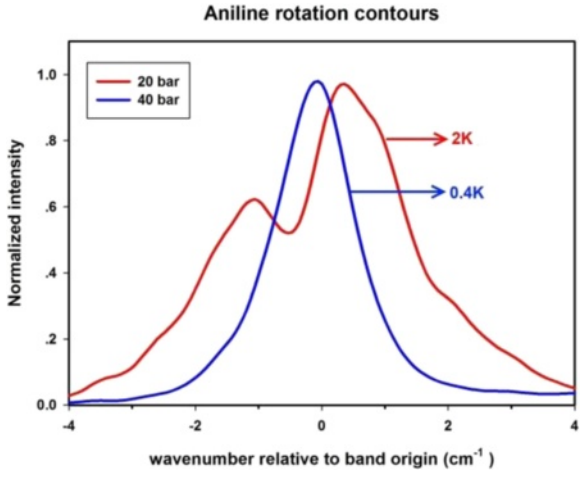

Fig. 22 Rotational line profile of Aniline 0–0 origin in helium gas jet with estimated temperature from spectral calculation [61]

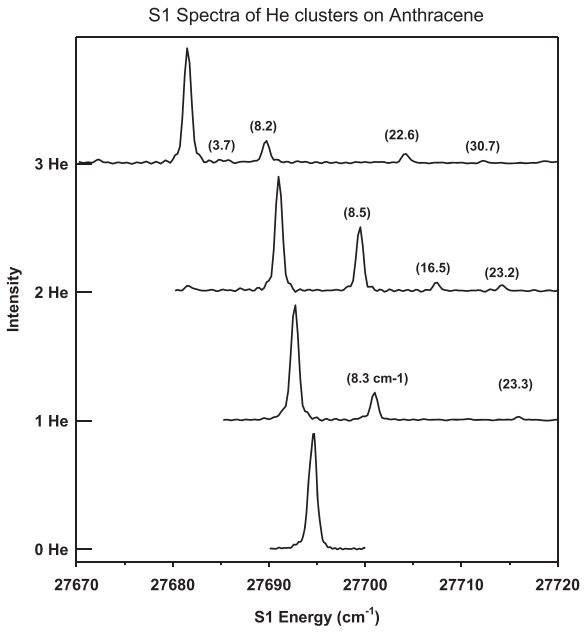

Fig. 23 Spectra of helium clusters on Anthracene indicating the low temperatures achieved (less than 0.8 K) [21]

The heavier gases cannot produce very cold beams as they tend to form clusters [12]. While helium can be cooled down to 10 mK [12], krypton and argon are limited to ~1 K only.

The onset of clustering can be quite abrupt as can be seen in Fig. 21, where we measured the scattered laser light (266 nm) near the nozzle as we cooled the valve. Helium droplets can easily be produced when the valve is cooled below 20 K [22].

If we seed the carrier gas with heavier (organic) molecules, they can be cooled down in the beam to less than 1 K [39–41] as we measured the rotation line width of the seeded molecule (see Figs. 22 and 23).

Skimmer design and position

Because high pressure shaped nozzles can produce high on-axis beam intensities, it is not surprising that modifications of the accepted skimmer design are required. Since the early days of low intensity continuous beams, skimmers have been recognized as more than a simple bystander that extracts the central portion of the beam. The effects of molecules scattering from the finite skimmer edges have long been recognized [1, 5, 31, 42–44], and the reduced transmission of the beam through the skimmer was termed "skimmer interference". At times the term "skimmer clogging" was used to describe the dramatic reduction in skimmer transmission. To study these effects, we employed the same DSMC gas flow simulation program [32] which is eminently suitable for the gas density encountered at the skimmer. Here we show how the skimmer distance, skimmer opening, and skimmer edge sharpness influence the transmission of the beam through the skimmer.

We begin by examining a popular skimmer shape that was used extensively in low intensity continuous beams [45]. The skimmer opening is 1 mm. and its length is

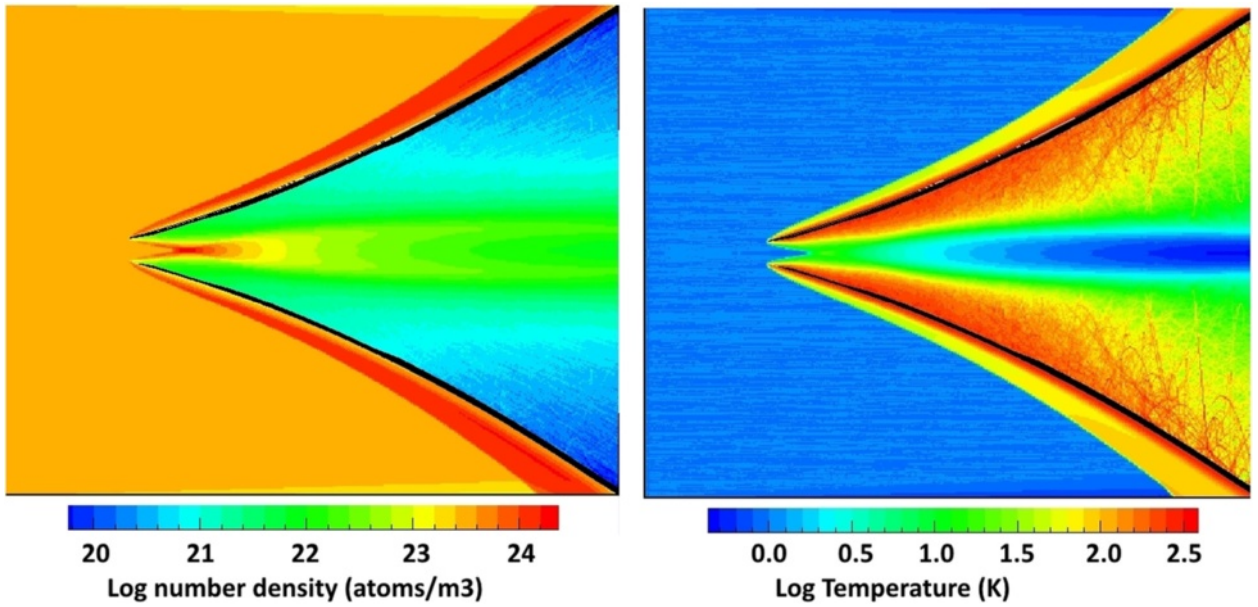

Fig. 24 Density and temperature maps near a trumpet shape skimmer when subjected to high number density of 10^{23} atoms/m^3 cold neon beam. The skimmer is completely clogged

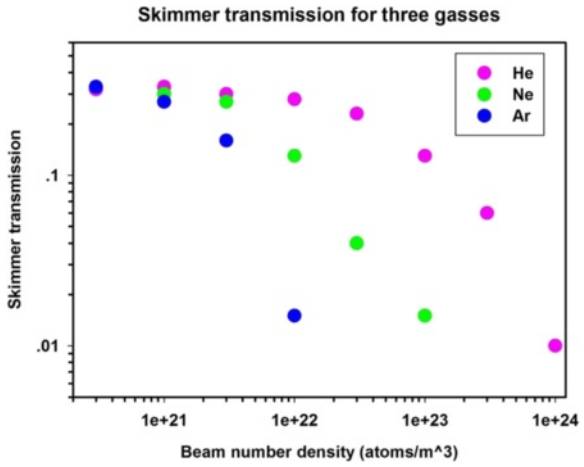

Fig. 25 Skimmer transmission as a function of incoming beam gas density, for the skimmer depicted in Fig. 24

22 mm. The included full angle at its tip is 25^0 and at its base 70^0. The tip sharpness is determined by the simulation mesh size and is ~ 5 micometers. The simulation represents the flow of a collimated and cold stream of neon at 1 K moving at 750 m/s to the right. We chose the neon beam number density ($3*10^{23}$ atoms/m^3) to represent the density of the gas from a 0.2 mm. conical nozzle at a stagnation pressure of 30 bar and at a distance of 10 mm from the nozzle (extrapolated from Fig. 3). Figure 24 represents a clogged skimmer condition with a high density gas plug formed at the skimmer throat, serving as a secondary expansion point from this higher temperature plug (25 K). The transmitted beam intensity at the skimmer base is less than 2 % of the incoming beam number density.

It is obvious from the simulation that the skimmer shape is wrong and that the entering beam intensity is too high. A severe loss of beam intensity is caused by the shock wave structure near the skimmer entrance.

Skimmer clogging, and therefore low beam transmission, can occur quite suddenly as the gas beam density rises. This effect is illustrated in Fig. 25, where skimmer transmission as a function of beam gas density is plotted for the skimmer

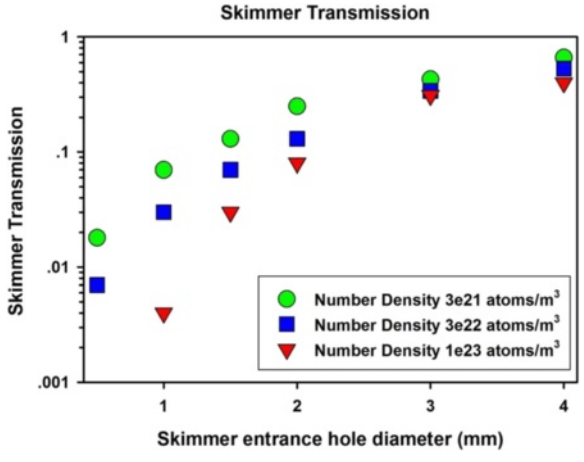

Fig. 26 Skimmer transmission as a function of skimmer aperture (diameter) and beam density [62]. Simulations are for argon, where full energy accommodation is assumed

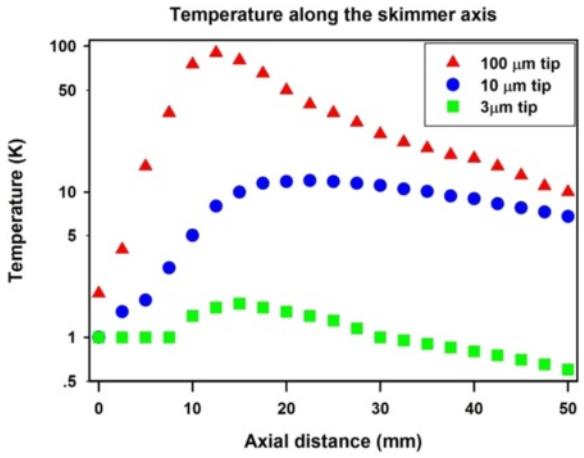

Fig. 27 Temperature rise in a blunt skimmer [62]. The flowing gas is neon (energy accommodation coefficient 0.8) at 1 K and a number density of 10^{22} atoms/m^3. Skimmer entrance aperture is 1 mm. The Temperature of the gas rises for only few ms at the skimmer entrance, but this can destroy fragile clusters

described above and illustrated in Fig. 24. In Fig. 25, skimmer transmission is defined as the ratio of the gas number density at the skimmer outlet to the density at the skimmer inlet. The simulation results are sensitive to the interaction parameters of the gas with the skimmer surface (energy accommodation occurring in the gas surface collision). The accommodation coefficient rises as the mass of the gas atoms approaches that of the surface atoms (Nickel). We chose accommodation coefficients of 0.4 for He, 0.8 for Ne and 1 (complete accommodation) for Ar [46].

A surprising result is that in order to allow for a reasonable beam transmission one has to move the skimmer to a larger distance from the nozzle, as large as 150 mm. (or 750 nozzle diameters!) for Ne or 55 mm. for helium. Lower beam transmission is found for Ar.

The next issue we address is the how does the skimmer entrance hole affects its transmission. The simulations shows that smaller hole skimmer tend to clog up at lower beam densities than a larger entrance hole skimmers (Fig. 26).

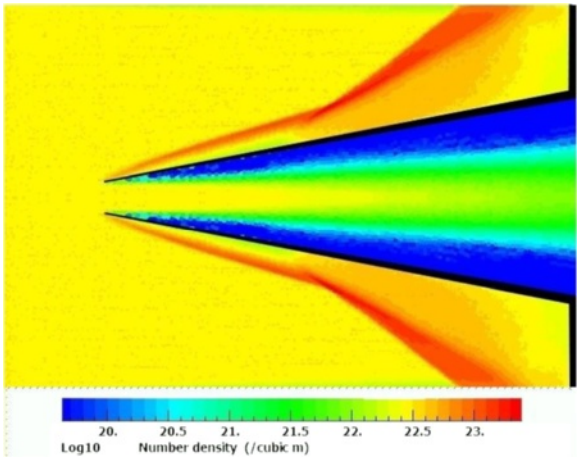

Fig. 28 Slim (20^0 full opening angle) conical skimmer transmission. Helium at 1 K is flowing to the right. Helium number density is 10^{22} atoms/m^3

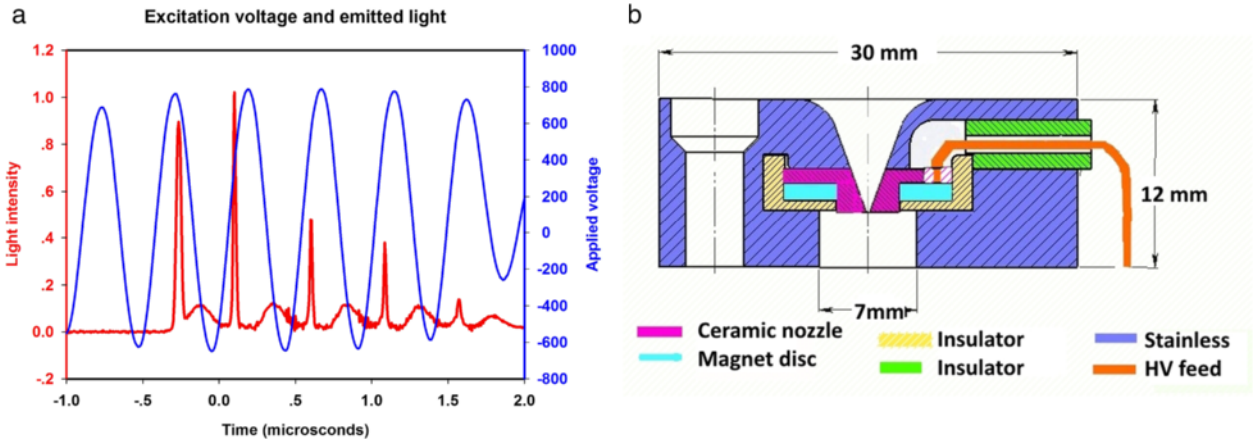

Fig. 29 a: Excitation waveform high voltage burst (1Kv at 0.5 microseconds. spacing). Notice the short duration of the light (current) pulses. **b**: Cross section of the DBD electrode. The high voltage pulses are applied to the magnet disc outside the ceramic nozzle

To achieve the best transmission results, it is necessary to employ a large diameter entrance aperture (2–4 mm) and to move the skimmer by as much as 1000 nozzle diameters downstream from the nozzle (100–200 mm) to avoid strong beam attenuation in the skimmer. This is illustrated in Fig. 27, where the skimmer transmission is plotted as a function of skimmer entrance diameter for conical skimmers (20° full opening angle) subjected to gas densities ranging from 3×10^{21} to 1×10^{23} atoms/m^3. The necessity of using narrow conical skimmers with large diameter entrance apertures, positioned far downstream is a very unorthodox result that will require the redesign of source chambers for a large number of currently employed high intensity supersonic sources.

The last question we wish to address is how sharp does the skimmer edge need to be? We can simulate the temperature rise of the cold beam due to molecules scattering from the room temperature skimmer edges. The results are shown in Fig. 28. A long conical skimmer was used and the axial temperature along its axis is shown. Beam number density is 10^{22} of helium. A wall thickness of 3 μm causes little beam heating in the skimmer. A 10 μm tip thickness is already causing significant beam heating, and a 100 μm wall is simply bad. Sharply honed or electro polished edges can be machined on the skimmer tip to an edge that is smaller than 3 microns. Slit skimmer based on honed razors can be even sharper.

Ionic clusters and radical sources

There are some experiments where we want to study ions, ionic clusters, meta-stable atoms or molecular radicals. There were several attempts to combine a nozzle with electrical or laser discharge scheme to produce these species. In most cases the excitation process warms the supersonic jet, or contaminates it with sputtered electrode material [47–52]. We have developed a new type of electrode less Dielectric Barrier Discharge [53–56] source that does not heat the jet or contaminates it [57]. The source is attached to the front flange of the Even-Lavie valve and uses a built in disk magnet to confine the discharge electrons. It operates on a series of rapid high voltage pulses.

The basic idea is that the current in the discharge is limited by the dielectric barrier charging to very short current spikes (nano-sec. duration), not allowing for an arc to form during the avalanche breakdown (Figs. 29 and 30).

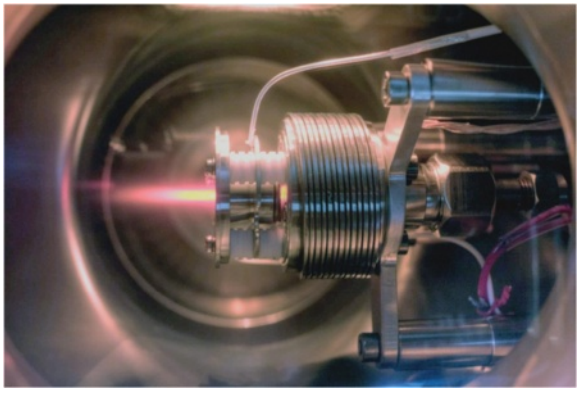

Fig. 30 Excited neon flame coming from the DBD discharge. The beam remains collimated and cold

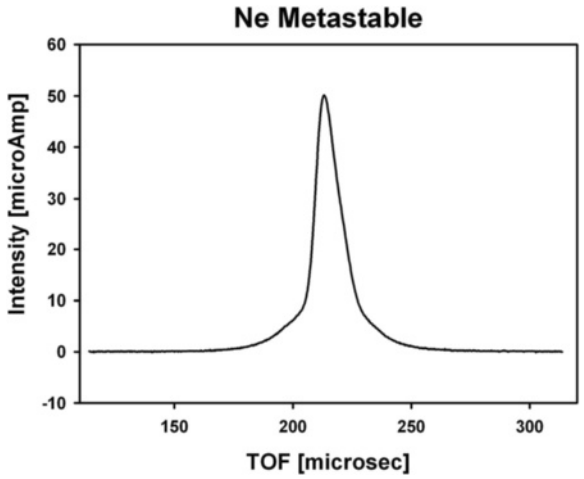

Fig. 31 Meta-stable caused current collected on a plate that is placed after the skimmer at 250 mm distance from the valve. Mach number of ~50

This type of excitation is highly reproducible and is stable for millions of pulses. No sign of sputtering or electrode erosion was noticeable. Several species can be generated in the discharge. The most obvious are excited meta- stable atoms (Fig. 31).

The high collected current represents very high flux ($3*10^{14}$ atoms/second, at the peak, for a time duration of ~10 microseconds). The narrow time width indicates high Mach number of the beam (up to 50) so no appreciable heating of the beam occurs [35, 58, 59]. The excitation occurs inside the expansion nozzle where there are still many collisions in the gas. The meta-stable energy state is the lowest excited state of the atoms. When using gas mixture we find only the lowest meta-stables. Thus a mixture of helium and neon will produce only the neon excited atoms. Even trace impurities (10 ppm) will steal the energy from the excited helium and transfer it to lower molecular states with high efficiency. Water is a common impurity and needs to be removed if meta-stable Helium is to be created efficiently.

When molecules, with lower ionization potential than that of the carrier gas metastable energy (almost all molecules), than the dominant species that are created are molecular ions or fragmented radicals. This is shown in Fig. 32.

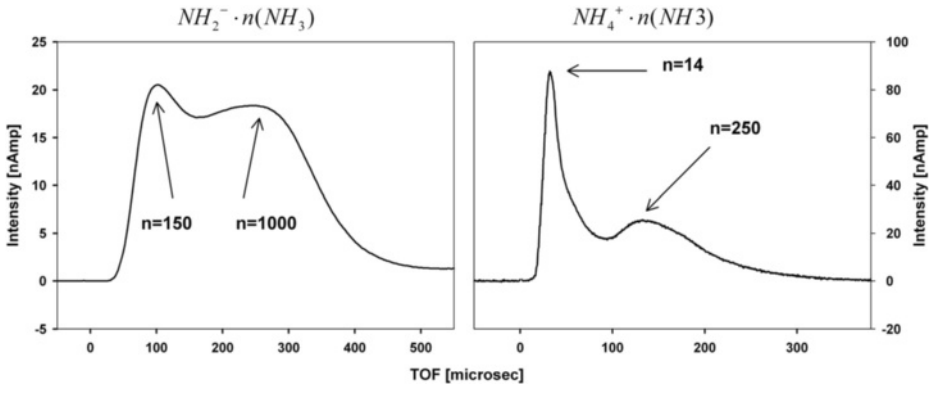

Fig. 32 positive and negative ion mass spectra of large (and unresolved) ammonia clusters (positively and negatively charged) produced by the DBD discharge of 3 % ammonia in helium carrier gas at 80 Bars

This DBD source can replace laser photo fragmentation in many cases, with the added advantage of producing cold jets.

Conclusions

We have shown that intense and cold (<10mK) pulsed jets of short durations (25micro-sec.) and high repetition rate can be produced. The high pressure used in the valve and some nozzle shaping contribute to the beam intensity. Changes in skimmer shape and positioning are required to take advantage of the higher beam intensities.

Competing interests
The authors declare that they have no competing interests.

Received: 19 November 2015 Accepted: 16 December 2015
Published online: 29 December 2015

References

1. N. F. Ramsey, (Oxford University Press, Oxford, 1956).
2. Ashkenas H, Sherman SF (1966) Proceedings of the 4th International Symposium on Rarefied Gas Dynamics: Experimental Methods in Rarefied Gas Dynamics. Academic, New York
3. Hagena OF, Obert W (1972) Cluster Formation in Expanding Supersonic Jets: Effect of Pressure, Temperature, Nozzle Size, and Test Gas. J Chem Phys 56(5):1793
4. Smalley RE, Wharton L, Levy DH (1977) Molecular Optical Spectroscopy with Supersonic Beams and Jets. Acc Chem Res 10:139
5. Campargue R (1980) Characteristics of Supersonic Beams Applicable in Collision or Semi-Collision Experiments. J Chim Phys Pcb 77(3):R15
6. Toennies JP, Winkelman K (1977) Theoretical studies of highly expanded free jets: Quantum effects. J Chem Phys 66(9):3965
7. Campargue R (1984) Progress in Overexpanded Supersonic Jets and Skimmed Molecular Beams in Free-Jet Zones of Silence. J Phys Chem 88:4466–4414
8. Scoles G (1988) Atomic and Molecular Beam Methods. Oxford University Press, New York, Oxford
9. Haberland H (1994) Clusters of Atoms and Molecules. Springer, Berlin
10. Gentry WR, Giese CF (1978) Ten microsecond pulsed molecular beam source and a fast ionization detector. Rev Sci Instrum 49:595
11. Even U, Bahat D, Cheshnovsky O, Lavie N, Magen Y (1987) Generation and Detection of Intense Cluster Beams. J Phys Chem 91(10):2460
12. Hillenkamp M, Keinan S, Even U (2003) Condensation limited cooling in supersonic expansions. J Chem Phys 118(19):8699–8705
13. Yan B, Claus PFH, Oorschot BGMv, Gerritsen L, Eppink ATJB, Meerakker SYTvd, Parker DH (2013) A new high intensity and short-pulse molecular beam valve. Review of Scientific Instruments 84:023102
14. in Parker pulsed valves (http://ph.parker.com/us/12051/en/pulse-valves-miniature-high-speed-high-vacuum-dispense-valve).
15. Irimia D, Dobrikov D, Kortekaas R, Voet H, Ende DAvd, Groen WA, Janssen MH (2009) In situ characterization of a cold and short pulsed molecular beam by femtosecond ion imaging. Rev Sci Instrum 8(11):113303
16. Vogels SN, Gao Z, Meerakker SYvd (2015) Optimal beam sources for Stark decelerators in collision experiments: a tutorial review. EPJ Techniques and Instrumentation 2:12
17. Even U (2014) Pulsed Supersonic Beams from High Pressure Source: Simulation Results and Experimental Measurements. Advances in Chemistry 2014:636042
18. Lorentz. (https://www.integratedsoft.com/products/lorentz).
19. Scilab. (http://www.scilab.org/).
20. Christen W (2013) Stationary flow conditions in pulsed supersonic beams. J Chem Phys 139:154202
21. Even U, Al-Hroub I, Jortner J (2001) Small He clusters with aromatic molecules. J Chem Phys 115(5):2069
22. Pentlehner D, Riechers R, Dick B, Slenczka A, Even U, Lavie N, Brown R, Luria K (2009) Rapidly pulsed helium droplet source. Rev Sci Instrum 80:043302
23. Mudrich M, Stienkemeier F (2014) Photoionizaton of Pure and Doped Helium Nanodroplets. International Reviews in Physical Chemistry 33(3):301
24. A. I. G. Flórez, D.-S. Ahn, S. Gewinner, W. Schöllkopf and G. v. Helden, Physical Chemistry Chemical Physics (34) (2015)
25. Pedemonte L, Bracco G, Tatarek R (1999) Theoretical and experimental study of He free-jet expansions. Phys Rev A 59(4):3084
26. Tafreshi HV, Benedek G, Piseri P, Vinati S, Barborini E, Milani P (2002) A Simple Nozzle Configuration for the Production of Low Divergence Supersonic Cluster Beam by Aerodynamic Focusing. Aerosol Science and Technology 36:593–606
27. Semushin S, Malka V (2001) High density gas jet nozzle design for laser target production. Rev Sci Instrum 72(7): 2961
28. J. T. McDaniels, R. E. Continetti and D. R. Miller, in *Rarefied Gas Dynamics*, edited by A. D. Ketsdever (American Institute of Physics, 2003), Vol. 23rd international symposium.

29. Schmid K (2009) Dissertation. 2009 Supersonic Micro-Jets And Their Application to Few-Cycle Laser-Driven Electron Acceleration. Ludwig–Maximilians–Universität
30. H. Pauli, Atoms, Molecules, and Cluster Beams I. (Springer-Verlag Berlin, 2000)
31. Braun J, Day PK, Toennies JP, Wittec G, Neher E (1997) Micrometer-sized nozzles and skimmers for the production of supersonic He atom beams. Rev Sci Instrum 68(8):3001
32. Bird G. (http://www.gab.com.au/).
33. He X, Feng X, Zhong M, Gou F, Deng S, Zhao Y (2014) The influence of Laval nozzle throat size on supersonic molecular. Mod J Transport 22(2):118
34. Bird GA (1994) Molecular Gas Dynamics and the Direct Simulation of Gas Flows. OUP, Oxford
35. Shagam Y, Narevicius E (2013) Kelvin Collision Temperatures in Merged Neutral Beams by Correlation in Phase-Space. J Phys Chem C 117:22454
36. Henson AB, Gersten S, Shagam Y, Narevicius J, Narevicius E (2012) Observation of Resonances in Penning Ionization Reactions at Sub-Kelvin Temperatures in Merged Beams. Science 338:234
37. Osterwalder A (2015) Merged neutral beams. EPJ Tech Instrum 2:10
38. Jankunas J, Jachymski K, Hapka M, Osterwalder A (2015) Observation of orbiting resonances in He((3)S(1)) + NH3 Penning ionization. J Chem Phys 142:164305
39. Even U, Jortner J, Noy D, Lavie N, Cossart-Magos C (2000) Cooling of large molecules below 1k and He Clusters. J Chem Phys 112(18):8068
40. Stapelfeldt H (2004) Laser Aligned Molecules: Applications in Physics and Chemistry. Physica Scripta T T110:132
41. Holmegaard L, Nielsen JH, Nevo I, Stapelfeldt H, Filsinger F, Kupper J, Meijer G (2009) Laser-Induced Alignment and Orientation of Quantum-State-Selected Large Molecules. Phys Rev Letters 102(2):023001
42. Bailey AB, Dawbarn R, Busby MR (1976) Effects of Skimmer and Endwall Temperature of Condensed Molecular Beams. Journal of AIAA 14:1
43. Gentry WR, Giese CF (1975) High-precision skimmers for supersonic molecular beams. Rev Sci Instrum 46(1):104
44. Jordan DC, Barling R, Doak RB (1999) Refractory graphite skimmers for supersonic free-jet, supersonic arc-jet, and plasma discharge applications. Rev Sci Instrum 70(3):1640
45. Beam-Dynamics, (http://www.beamdynamicsinc.com/skimmer_specs.htm).
46. D. J. Rader, W. M. Trott, J. R. Torczynski, J. N. Castañeda and T. W. Grasser, Sandia National Laboratories SAND2005-6084, http://prod.sandia.gov/techlib/access-control.cgi/2005/056084.pdf (2005).
47. Ren Z, Qiu M (2006) DD Li Che. X Wang, X Yanga A double-stage pulsed discharge fluorine atom beam source Rev Sci Instrum 77:016102
48. Lu IC, Huang WJ, Chaudhuri C, Chen WK, Lee SH (2007) Development of a stable source of atomic oxygen with a pulsed high-voltage discharge and its application to crossed-beam reactions. Rev Sci Instrum 78(8):083103
49. Rennick CJ, Morrison JP, Ortega-Arroyo J, Godin P, Grant ER (2009) Charge, density and electron temperature in a molecular ultracold plasma. Chemical Physics arXiv:0911.0466 [physics.chem-ph]
50. Woestenenk GR, Thomsen JW, Rijnbach M, Straten P, Niehaus A (2001) Construction of a low velocity metastable helium atomic beam. Rev Sci Instrum 72(10):3842
51. Verheien MJ, Beierinck HCW, Renes WA, Verster NF (1984) A double differentially pumped supersonic secondary beam. J Phys, E: Sci Instrum 17:1207
52. Halfmann T, Koensgen J, Bergmann K (2000) A source for a high-intensity pulsed beam of metastable helium atoms. Meas Sci Technol 11:1510
53. Kogelschatz U (2003) Dielectric-Barrier Discharges: Their History, Discharge Physics, and Industrial Applications. Plasma Chemistry and Plasma Processing 23(1):1
54. Massines F, Segur P, Gherardi N, Khamphan C, Ricard A (2003) Physics and chemistry in a glow dielectric barrier discharge at atmospheric pressure. Surf Coat Technol 174:8
55. Bednar N, Matovic J, Stojanovic G (2013) Properties of surface dielectric barrier discharge plasma generator for fabrication of nanomaterials. J Electrostatics 71:1068
56. Kazanskiya NL, Kolpakova VA, Podlipnova VV (2014) Gas discharge devices generating the directed fluxes of off-electrode plasma. Vacuum 101:291
57. Luria K, Lavie N, Even U (2009) Dielectric barrier discharge source for supersonic beams. Rev Sci Instrum 80:104102
58. Lavert-Ofir E, Shagam Y, Henson AB, Gersten S, Klos J, Zuchowski PS, Narevicius J, Narevicius E (2014) Observation of the isotope effect in sub-kelvin reactions. Nat Chem 6(4):332
59. Bergeat A, Onvlee J, Naulin C, Avoird A, Costes M (2015) Quantum dynamical resonances in low-energy CO(j = 0) + He inelastic collisions. Nat Chem 7:349
60. Belan M, Ponte SD, Tordella D (2010) Highly underexpanded jets in the presence of a density jump between an ambient gas and a jet. Phys Rev E 82(2):026303
61. Amirav A, Even U, Jortner J (1983) FW Birss. DA Ramsay Rotational cooling of aniline in axis-symmetric and planar pulsed supersonic expansions Canad J Phys 61:278
62. Even U, Christen W, Luria K, Rademann K (2011) Generation and Propagation of Intense Supersonic Beams. J Phys Chem A 115:7362